# Microwave Imaging via Distorted Iterated Virtual Experiments and Compressive Sensing

Roberta Palmeri, *Student Member, IEEE,* Martina T. Bevacqua, *Student Member, IEEE,* Lorenzo Crocco, *Senior Member, IEEE,* Tommaso Isernia, *Senior Member, IEEE*, and Loreto Di Donato, *Member, IEEE*

***Abstract*— The linearity of the scattering phenomenon with respect to primary sources allows to recombine a posteriori the available experiments and build, in a synthetic fashion, new '*virtual*' experiments. Starting from this circumstance, an iterative procedure is proposed as an effective approach to tackle non linear inverse scattering problems. In this procedure, the Green's function, the virtual experiments and the corresponding field approximations are updated at each iteration. The structure and the complexity of the approach are comparable with those of the widely adopted distorted Born iterative method, but its performances are remarkably better, thanks to extended validity of the exploited field approximation. The overall approach also takes advantage of a Compressive Sensing based regularization scheme to further improve the accuracy of the imaging results. Examples with numerical and experimental data are given to assess the method.**

***Index Terms*— Inverse Scattering, Distorted Born Iterated Method, Virtual Experiments, Compressive Sensing, Linear Sampling Method, Truncated Singular Value Decomposition.**

## I. Introduction

MICROWAVE imaging techniques are an active research topic in applied electromagnetics, owing to their relevance in both theory and applications. In this framework, one of the main still open challenges is to develop methods and techniques capable to overcome the difficulties arising from the non-linearity and ill-posedness of the underlying inverse scattering problem [1,2].

As a countermeasure to non-linearity, Born, Rytov, and Kirchhoff [2-4] field approximations, have been exploited to linearize the problem and solve it in an efficient and simple way. However, this is only possible within the (limited) validity of the underlying linear models. For example, the Born approximation (BA) is viable only for the weak scattering regime [1-3]. Similar limitations hold for the distorted Born approximation (DBA) [5], where one looks for the perturbations in a known inhomogeneous scenario.

A possible extension of DBA to the case of non-weak scatterers is the distorted Born iterative method (DBIM) [6-13], which consists of iterated linear approximations, achieved by progressively updating the scenario (i.e., the relevant Green function and the total field) and looking for the perturbation. Obviously, the final outcome depends on the starting guess as well as on the range of validity of the intermediate linearizations.

Notably, it can be argued that the wider the range of validity of the approximations, the larger the possibility to recover the actual (ground truth) contrast profile. In fact, at any iteration the approach will more easily contain the actual solution within its range of validity. Also, it will more easily include points belonging to the attraction region of the actual solution.

Hence, it makes sense to look for field approximations having a validity range as broad as possible. In this respect, the field conditioning enforced by means of suitably designed *virtual experiments* (VE) [14-16] is worth to be considered. In fact, the VE allow to introduce a new, "scatterer aware", field approximation [14], which is viable for a large class of non-weak targets [15], as well as for the case of partially known scenarios [17].

Then, in the same spirit as DBIM, we introduce and develop in the following a new iterative inversion scheme. In each iteration of this latter, after the scenario's update, the VE are also re-designed, thus allowing convenient VE based linear approximations. By so doing, each step relies on a linear approximation with an extended validity (as compared to DBA). In fact, the nature of the scatterer is somehow taken into account. As such, the resulting *Distorted Iterated Virtual Experiments* (DIVE) scheme is expected to be more robust than DBIM.

Obviously, in each step of DIVE, one still has to face an ill-posed (linear) inverse problem, which requires a regularization to obtain physically meaningful solutions. To this end, we consider two possible strategies. The first is a "general purpose" approach, based on the truncated singular value decomposition (TSVD) [14], which allows us to assess the effectiveness of the basic idea underlying DIVE. The second is based on the Compressive Sensing (CS) theory [18-20], already exploited in inverse scattering when using BA [21,22] or DBIM [11,12]. In this paper, we exploit it into DIVE as a

This is the postprint version of the following article: R. Palmeri, M. T. Bevacqua, L. Crocco, T. Isernia and L. Di Donato, "Microwave Imaging via Distorted Iterated Virtual Experiments," in IEEE Transactions on Antennas and Propagation, vol. 65, no. 2, pp. 829-838, Feb. 2017, doi: 10.1109/TAP.2016.2633070. Article has been published in final form at: https://ieeexplore.ieee.org/document/7762747.

regularization strategy for objects exhibiting piece-wise constant permittivity distributions.

The paper is organized as follows. In Section II, the basic mathematical formulation of the inverse scattering problem and the VE framework are recalled. In Section III, the proposed iterative procedure is introduced and described in detail, while in Section IV the inversion strategies exploited for the solution of the linear ill-posed problem involved in each iteration are outlined. Section V presents the assessment of the DIVE method's performance with benchmark numerical and experimental data. The results fully confirm the expectations and demonstrate it as a reliable and effective imaging tool for the non-weak scattering regime. Conclusions follow.

Throughout the paper we consider the canonical 2D scalar problem (TM polarized fields) and we assume and drop the time harmonic factor $exp\{j\omega t\}$.

## II. Mathematical Basics and the VE Framework

Let Ω denote the compact, possibly not connected, support of an unknown object with relative permittivity $\varepsilon_s$ and electric conductivity $\sigma_s$. The object is embedded in a homogeneous medium with permittivity $\varepsilon_b$ and conductivity $\sigma_b$. The magnetic permeability is everywhere equal to that of the free space $\mu_0$. The relevant contrast function is defined as:

$$\chi(\boldsymbol{r}) = \frac{\varepsilon_s(\boldsymbol{r}) - j\sigma_s(\boldsymbol{r})/\omega\varepsilon_0}{\varepsilon_b - j\sigma_b/\omega\varepsilon_0} - 1 \tag{1}$$

where $\boldsymbol{r} = (x, y) \in \Omega$ and $\omega = 2\pi f$ with $f$ the working frequency.

The unknown scatterer is probed with a set of incident fields transmitted by some antennas located in $\boldsymbol{r_t}$ on a closed curve Γ. Without any loss of generality, let us assume that the scattered fields are measured by means of receiving antennas at $\boldsymbol{r_m} \in \Gamma$.

Under the above, the equations describing the scattering problem can be expressed as:

$$E_s(\boldsymbol{r_m}, \boldsymbol{r_t}) = k^2 \int_\Omega G_b(\boldsymbol{r_m}, \boldsymbol{r'})\, \chi(\boldsymbol{r'}) E(\boldsymbol{r'}, \boldsymbol{r_t}) d\boldsymbol{r'} = \mathcal{A}_e[\chi E] \tag{2}$$

$$E(\boldsymbol{r}, \boldsymbol{r_t}) = E_i(\boldsymbol{r}, \boldsymbol{r_t}) + k^2 \int_\Omega G_b(\boldsymbol{r}, \boldsymbol{r'})\, \chi(\boldsymbol{r'}) E(\boldsymbol{r'}, \boldsymbol{r_t}) d\boldsymbol{r'} = E_i + \mathcal{A}_i[\chi E] \tag{3}$$

where $E_i$, $E_s$ and $E$ are the incident, scattered and total field, respectively, $k = \omega\sqrt{\mu_b \varepsilon_b}$ is the wavenumber in the host medium, $G_b$ is the Green's function pertaining to the background medium. If the background is the free space $G_b(r, r') = -j/4\, H_0^2(k_b|r - r'|)$, being $H_0^2$ the zero order and second kind Hankel function. In general case of non homogenous background, $G_b$ cannot be calculated in closed form, except for some canonical scenarios. Finally, $\mathcal{A}_e$ and $\mathcal{A}_i$ are a short notation for the integral external and internal radiation operators, respectively.

The inverse scattering problem consists in estimating the contrast function $\chi$ from the (noise corrupted) measured scattered field $E_s$. Due to the properties of the involved operators, such a problem is ill posed [2] and non-linear, as the total field also depends on the unknown contrast. The standard DBIM, originally proposed by Chew and Wang [6], overcomes this difficulty by considering a series of intermediate linearizations. In each step, it involves the solution of a forward problem to update the background field as well as the relevant Green's function. The final outcome strongly depends on the initial guess and on the range of validity of the intermediate linearizations.

### A. The virtual experiments framework

In the above formulation of the inverse scattering problem, multiple experiments have been considered to increase as much as possible the amount of independent information and improve the performances of the inversion strategy. However, due to ill-posedness, only a finite number of independent experiments is available [23]. That is, increasing the number of incidence directions (and, by reciprocity, of measurement positions) is only useful up to some extent. The number N (M) and the positions on Γ of the transmitting (receiving) probes can be properly chosen in a non-redundant fashion by relying on theoretical arguments [23].

The collected independent information can be re-organized by taking advantage of the linearity of the scattering phenomena. In fact, a linear combination of the incident fields, (with known coefficients) gives rise to a scattered field given by the linear combination (ruled by the same weighting coefficients) of the corresponding scattered fields. Starting from this simple "transformation" of the scattering data, the concept of VE has been introduced and exploited in [14-16]. Notably, the VE represent a re-arrangement of the original experiments, so that they do not require additional measurements, but can possibly provide a more convenient way to handle the inverse problem.

## III. DIVE - Distorted Iterated Virtual Experiments

The idea of transforming the original experiments into new (virtual) ones in such a way that the scattered fields exhibit a given behavior has opened the way to a number of interesting possibilities.

In particular, in [14] suitably designed VE and a new approximation for the internal fields have been introduced and described for the case of a homogeneous background. Herein, in the same spirit of DBIM, we pursue the idea of exploiting this approximation (rather than BA and DBA) as the core of an iterative procedure, which involves successive linearizations. Unlike DBIM, each linearization of DIVE is based on properly re-designed VE, which are updated on the basis of intermediate results.

The new procedure is articulated in five steps.

1) *Initialization:* a first estimation $\chi^1$ of the contrast function is obtained by using the VE based linear approximation [14].

Obviously, the proposed iterative procedure can consider other more favorable starting guesses, when available.

2) *Scenario update*: the forward scattering problem pertaining to the last reconstructed contrast profile $\chi^k$, which represents the background medium at the $k^{th}$ iteration, is solved. Such a solution allows to update the background field ${E_b}^k$, that is, the total field occurring when $\chi = \chi^k$, and the anomalous field $\Delta {E_s}^k$ (that is, the difference between $E_s$ and the field scattered when $\chi = \chi^k$). Furthermore, the Green's function ${G_b}^k$ pertaining to the achieved estimation of the background permittivity is also computed, by using reciprocity.

*3) Convergence control:* a stopping rule is considered by defining the relative residual error (RRE) at $k^{th}$ iteration as $RRE^k = \|\Delta {E_s}^k\|_2 / \|E_s\|_2$. If $RRE^k$ is less than a pre-set threshold ($10^{-5}$) or is larger than the $RRE^{k-1}$, the procedure is stopped and $\chi^k$ is considered the solution of the overall problem. Otherwise, the iterative procedure continues until the stopping criterion is fulfilled.

*4) VE update*: this step and the following one are the main and most important differences between DBIM and DIVE. In fact, we consider new Virtual Experiments, which are re-designed in such a way to focus the anomalous field only in those points where perturbations, say $\Delta\chi^k$, with respect to the last reconstructed profile ( $\chi^k$) are expected. To this end, we solve in each sampling point $\boldsymbol{r_s}$ the (distorted) linear sampling method (LSM) equation [24,25]:

$$\sum_{t=1}^{N} \Delta {E_s}^k(\boldsymbol{r_t}, \boldsymbol{r_m}) \alpha^k(\boldsymbol{r_t}, \boldsymbol{r_s}) = {G_b}^k(\boldsymbol{r_m}, \boldsymbol{r_s}) \tag{4}$$

wherein $\alpha^k(\boldsymbol{r_t}, \boldsymbol{r_s})$ are the sought auxiliary excitations coefficients which allow a convenient design of the k[th] set of VE (see below). To solve eq. (4) and counteract its ill-posedness, the singular value decomposition (SVD) of $\Delta E_s$ and the Tikhonov regularization are exploited [2].

According to [24], the energy of the coefficients $\alpha^k$ provides an estimation of the shape of $\Delta\chi^k$. In particular, the support indicator $\Upsilon^k$ normalized over the sampling grid is defined as

$$\Upsilon^k(\boldsymbol{r_s}) = \frac{log_{10}\|\alpha^k\| - log_{10}\|\alpha^k\|_{max}}{min\{log_{10}\|\alpha^k\| - log_{10}\|\alpha^k\|_{max}\}} \tag{5}$$

wherein $\|\cdot\|$ is the $\boldsymbol{\ell_2}$-norm.

Then, we select a number of *pivot* points $\boldsymbol{r_p}$ belonging to the estimated support of the anomaly to build the VE [14]. For instance, saying ${\mathcal{E}_b}^k$ the virtual background field, this is obtained by recombining ${E_b}^k$ through the coefficients $\alpha^k$, i.e.:

$${\mathcal{E}_b}^k(\boldsymbol{r}, \boldsymbol{r}_p) = \sum_{t=1}^{N} {E_b}^k(\boldsymbol{r}, \boldsymbol{r_t})\, \alpha^k(\boldsymbol{r_t}, \boldsymbol{r_p}) \tag{6}$$

*5) Contrast update via linear inversion:* the relevant data equation (1) is applied to the case of partially known scenario and recast in terms of VE as:

$$\Delta {\mathcal{E}_s}^k(\boldsymbol{r_m}, \boldsymbol{r_p}) = \int_{\Omega} {G_b}^k(\boldsymbol{r_m}, \boldsymbol{r'})\, \Delta\chi^k(\boldsymbol{r'}) \mathcal{E}^k(\boldsymbol{r'}, \boldsymbol{r_p}) d\boldsymbol{r'} = \mathcal{A_e}^{\boldsymbol{k}}[\Delta\chi^k \mathcal{E}^k] \tag{7}$$

where $\Delta {\mathcal{E}_s}^k$ and $\mathcal{E}^k$ are the anomalous and total fields arising in the VE, respectively, and $\mathcal{A_e}^{\boldsymbol{k}}$ is the external radiation operator at $k^{th}$ iteration.

By considering that the solution of eq. (4) enforces the scattered field to fit the elementary field pattern originating at the pivot point in the actual reference scenario [24,25], the unknown total field $\mathcal{E}^k$ in eq. (7) can be approximated by:

$$\mathcal{E}^k(\boldsymbol{r}, \boldsymbol{r}_p) = {\mathcal{E}_b}^k(\boldsymbol{r}, \boldsymbol{r}_p) + LP\{{G_b}^k(\boldsymbol{r}, \boldsymbol{r}_p)\} \tag{8}$$

i.e. by the sum of the virtual background field ${\mathcal{E}_b}^k$ and a low pass filtered version of ${G_b}^k$, as numerically computed by means of a forward solver. Note that approximation (8), unlike the DBA, takes into account the contribution of the anomaly through ${\mathcal{E}_b}^k$ at each step, so that it can be considered a "scatterer aware" approximation.

After solving the linearized problem (7) (see section V for details), a new profile is generated adding the reconstruction to the current reference scenario, that is $\chi^{k+1} = \chi^k + \Delta\chi^k$.

*6) Return to step 2*. The iteration continues until the stopping criterion is fulfilled.

The overall DIVE scheme is summarized in fig. 1.

## IV. TSVD and CS Based Inversion Strategies

In step 5), a linear ill-posed problem has to be solved. To this end, we consider two regularization approaches. The first approach is the well-known truncated singular value decomposition (TSVD) [2], whose regularization parameter, the truncation index $N_T$, can be conveniently determined by exploiting the Picard's plot technique [14,26,27]. We use this approach to prove the effectiveness of the VE iterations underlying the proposed method.

The second approach is based on the emerging Compressive Sensing (CS) paradigm [18-20]. In particular, let us suppose to deal with extended targets exhibiting piecewise constant dielectric profiles, which is a rather common circumstance when dealing with man-made objects and (some kind of) biological scenarios. Notably, they can be considered to be sparse when represented in terms of step functions. Alternatively, one can say that they have a gradient that is sparse in the usual pixel basis [28,29].

Let $\boldsymbol{D_h}$ and $\boldsymbol{D_v}$ be the vectors containing the horizontal and vertical forward differences [28,29] of the considered function. Moreover, in order to counteract, at least in a partial fashion, the (geometrical) anisotropy of more usual schemes

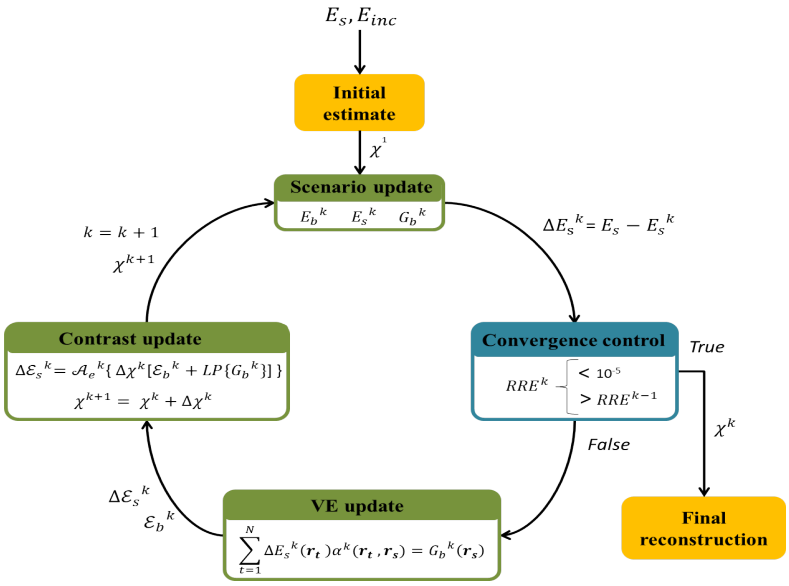


Fig. 1 The iterative scheme of DIVE method.

enforcing piecewise constant profiles, let us also define $\boldsymbol{D_d}^+$ and $\boldsymbol{D_d}^-$ as the vectors which contain the forward differences along directions parallel to the principal and secondary diagonal ($x = \pm y$) of the matrix of pixels representing a given function [29]. Accordingly, by paralleling [28], the linearized inverse problem can be solved by means of minimization of the following objective function:

$$\min_{\Delta\boldsymbol{\chi^k}} \left\{ \left\| \boldsymbol{D_h}\, \boldsymbol{\chi^{k+1}} \right\|_{\ell_1} + \left\| \boldsymbol{D_v}\, \boldsymbol{\chi^{k+1}} \right\|_{\ell_1} + \left\| \boldsymbol{D_d}^+ \boldsymbol{\chi^{k+1}} \right\|_{\ell_1} + \left\| \boldsymbol{D_d}^- \boldsymbol{\chi^{k+1}} \right\|_{\ell_1} \right\}$$
$$\textbf{subject to} \quad \left\| \boldsymbol{A^k} \Delta\boldsymbol{\chi^k} - \boldsymbol{y} \right\|_{\ell_2} \leq \delta \tag{9}$$

where $\boldsymbol{y}$ is the data vector containing the anomalous scattered fields $\Delta\mathcal{E}_s^k$ arising in the VE, and $\boldsymbol{A^k}$ is the matrix that relates the unknown vector to the data vector according to the linear relationship (7), with $\mathcal{E}^k$ given by expression (8).

A crucial point is the choice of the parameter $\delta$ in (9), which represents the level of accuracy required in satisfying (7). Of course, it has to take into account the noise level as well as the model error introduced by the approximation (8). In order to avoid the trivial solution, that is the null vector, $\delta$ must be selected lower than $\|\Delta\boldsymbol{\mathcal{E}_s}\|_{l_2}$, since with $\delta \geq \|\Delta\boldsymbol{\mathcal{E}_s}\|_{l_2}$ the null vector could satisfy the constraint on the data and simultaneously minimize the objective function. Accordingly, in performing the numerical analysis, $\delta$ is such that $\delta = \hat{\delta}\|\boldsymbol{\mathcal{E}_s}\|_{\ell_2}$ with $0 < \hat{\delta} < 1$. Moreover, since in the *Initialization* step a larger model error is expected, a larger value of $\delta$ is chosen with respect to the one adopted in the following steps.

Finally, it is worth to observe that while the TSVD regularization acts at each iteration on the perturbation $\Delta\boldsymbol{\chi^k}$, the CS inspired regularization in eq. (9) enforces sparsity on the whole contrast profile at each iteration. This is expected to improve the accuracy in the unknown profile reconstructions.

## V. Assessing DIVE Performances

### A. Synthetic data: the kite target

The imaging results in [14,15] show that the linear inversion method based on the approximation (8) can be applied in a range of cases much wider than the standard first order BA. On the other hand, the approach has anyway limitations with increasing the electrical dimensions (with respect to the background wavelength) and the contrast values of the scattering system [14]. Hence, to provide an assessment of DIVE, we have considered the 'kite' scatterer analyzed in [15], for which the VE based linear inversion fails. The leading dimension of the kite is 1 $\lambda_b$, being $\lambda_b$ the wavelength in the background, while the permittivity and the conductivity are, respectively, equal to 2.2 and 0.1 S/m at 5 GHz. The target is positioned inside a square domain of side L = 2.16 $\lambda_b$ discretized in 42 × 42 cells [30] (see fig. 3(a)-(b)). Moreover, following [23], 24 receivers and transmitters (both located on a circumference $\Gamma$ of radius R = 1.66 $\lambda_b$) have been considered. The scattered field data, simulated by means of a full-wave solver based on the method of moments, have been corrupted with a random Gaussian noise with SNR = 25 dB.

To evaluate the accuracy of the retrieved contrast function, we use the normalized mean square error defined by $err = \|\chi - \tilde{\chi}\|^2/\|\chi\|^2$, where $\chi$ is the actual contrast profile and $\tilde{\chi}$ the estimated one.

In fig. 2(c), the support indicator obtained in the *Initialization* step is shown. As it can be seen, the LSM is able to fairly identify the support of the target, thus allowing the selection of the pivot points and the design of the initial set of VE (k=1). As expected, the linear approximation fails. The corresponding TSVD reconstruction in shown in figs. 2(e)-(f). Nevertheless, this partial reconstruction is assumed as the new reference scenario and the pertaining forward scattering problem is solved. Then, the VE are updated on the basis of a new indicator, shown in fig 2(d), which allows to identify the support of the (geometrical and physical) variation $\Delta\chi^1$.

By iterating the design of VE, the proposed method in conjunction with TSVD is able to correct progressively the first reconstruction $\chi^1$ and finally obtain a satisfactory and quantitative reconstruction (err=18%) after a number of iterations equal to 7 (see figs 2(g)-(h)). Note that during the iterative procedure $N_T$ is set equal to [53,76,91,118,126,69,108,88], respectively.

For the sake of comparison, the same analysis has been performed by using the DBIM equipped with the same TSVD regularization (see fig. 2(i)-(l)). In this case, the iterative scheme diverges, with a reconstruction error of 199%. Since the Picard's plot cannot be safely exploited, because of the large model error associated to the DBA, some trial and error has been used to set the truncation index $N_T$, which has been finally set to the values where the singular values become 15 dB smaller than the first one.

The same analysis has been performed by using the CS approach to carry out the inversion at each iteration of DIVE. As it can be seen from figs. 2(m)-(p), the joint use of DIVE and CS provides a nearly optimal reconstruction, with a final reconstruction error as low as 3%. In this case, we have considered $\hat{\delta} = 0.75$ for the *Initialization* step and $\hat{\delta} = 0.55$ for the following iterations. Notably, the DBIM still diverges, even in conjunction with CS (err=120%).

For more details on the number of iterations, *err* and RRE relative to each method are reported in Table 1.

| | *err (k=0)* | *err* | *RRE* | *# iterations* |
|---|---|---|---|---|
| **DBIM-TSVD** | 1.00 | 1.99 | 0.194 | 3 |
| **DIVE-TSVD** | 0.89 | 0.18 | 0.005 | 7 |
| **DIVE-CS** | 0.76 | 0.03 | 0.003 | 7 |

Table 1. The kite target: details of the inversion procedure for different exploited approaches.

### *B. Experimental data: Fresnel database*

In this subsection we have considered three targets from the Fresnel database:

- *TwinDielTM*, which consists of two identical dielectric cylinders of radius 1.5 cm and relative permittivity 3 ± 0.3 [31];
- *FoamDielIntTM*, which is a piecewise inhomogeneous dielectric target made by two nested, non concentric, circular cylinders, where the inner one has a higher contrast (ε = 3 ± 0.3) than the outer one (ε = 1.45) [32];
- *FoamTwinDielIntTM*, in which another circular cylinder (ε = 3 ± 0.3) is placed in contact with the *FoamDielIntTM* target [32].

The complete description of the targets and the measurement set-up can be found in [31, 32]. Note the experiments have been carried out under a partially aspect limited configuration, where primary sources completely surround the targets, but, for each illumination, the measurements are taken only on an angular sector of 240°, that is, excluding a 120° sector centered on the incidence direction. In each example, the incident field has been estimated according to the calibration procedure in [16].

It is worth noting that all the reconstructions have been obtained using single frequency data. Besides being different from what is usually done in the literature (see for instance [8,33,34]), it is important to remark that the chosen frequency is such that the targets cannot be assumed to be "weak". In addition, no a priori information on the admissible values of permittivity and conductivity is enforced through regularization. Finally, to appraise the robustness of DIVE, we have also carried out an analysis when decreasing the number of data exploited in the quantitative inversion procedure. In particular, the reduction affects both the number of transmitting and receiving antennas, and the dimension of the processed data matrix is referred to as Z in Tables 2, 3 and 4.

For the *TwinDielTM* target, the working frequency is 6 GHz and the investigated area is 0.15x0.15 m$^2$. The results reported in fig. 3 have been achieved with $M \times N = 72 \times 36$. The outcome of the DIVE-TSVD approach is shown in figs. 3(b)-(c). As it can be seen, the method is able to retrieve the two cylinders. Nevertheless, the reconstruction with DIVE-CS (see figs. 3(d)-(e)) exhibits remarkable improvements, both in terms of electromagnetic properties and scatterers' shapes. Even when reducing experiments and data, using a $36 \times 18$ multiview-multistatic data matrix, the results are fully satisfactory, see figs. 3(f)-(g). For more details on the number of iterations and RRE relative to each method see Table 2.

For the *FoamTwinDielIntTM* target, the results are reported in fig. 4 and Table 3, repsectively. The working frequency is 4 GHz and the side of the investigated area is 0.175x0.175 m$^2$. Two size of the exploited multiview-multistatic data matrices are $45 \times 18$ and $23 \times 18$ respectively. Again, DIVE-CS gives back a more accurate reconstruction both in term of shape and electromagneties properties of the target (figs. 4(d)-(e),(f)-(g)) with respect to DIVE-TSVD (figs.4(b)-(c)).

Finally, for the *FoamDielIntTM* target, we have considered the data at 4 GHz and investigated a 0.125x0.125 m$^2$ domain. The results are reported in fig. 5 and have been achieved with $23 \times 18$ and $9 \times 9$ multiview-multistatic data matrices. DIVE-TSVD results are shown in figs. 5(b)-(c), while DIVE-CS ones in figs. 5(d)-(e),(f)-(g). As it can be seen, even in this case the improvements provided by the CS tool are obvious, as indeed DIVE-S is able to provide a nearly optimal reconstruction of the nominal electromagnetic properties of both the two nested cylinders. More details on the number of iterations, and the final value of RRE, are given in Table 4.

Note that in processing these data, we have used $\hat{\delta} = 0.40$ where a larger number of data is used and, so, a higher level of accuracy can be required, and $\hat{\delta} = 0.55$ in case of a reduced number of data. Finally, for the initial estimate of $\chi^1$ a value $\hat{\delta} = 0.75$ has been used.

In all cases, the iterative procedure stops because of the fulfillment of the convergence criterion in terms of RRE. For the sake of brevity, the unsuccessful inversions obtained with DBIM in the same conditions have not been reported.

| | *RRE* | *# iterations* |
|---|---|---|
| **DIVE-TSVD, Z=72x36** | 0.06753 | 12 |
| **DIVE-CS, Z=72x36** | 0.06826 | 5 |
| **DIVE-CS, Z=36x18** | 0.05374 | 7 |

Table 2. The Fresnel *TwinDielTM*: details of the inversion procedure.

| | *RRE* | *# iterations* |
|---|---|---|

| | | |
|---|---|---|
| **DIVE-TSVD, Z=45x18** | 0.01669 | 17 |
| **DIVE-CS, Z=45x18** | 0.01419 | 7 |
| **DIVE-CS, Z=23x18** | 0.09123 | 6 |

Table 3. The Fresnel *FoamTwinDielIntTM*: details of the inversion procedure.

| | | |
|---|---|---|
| **DIVE-TSVD, Z=23x18** | 0.0182 | 10 |
| **DIVE-CS, Z=23x18** | 0.0188 | 5 |
| **DIVE-CS, Z=9x9** | 0.0354 | 6 |

Table 4. The Fresnel *FoamDielIntTM*: details of the inversion procedure.

| | ***RRE*** | ***# iterations*** |
|---|---|---|

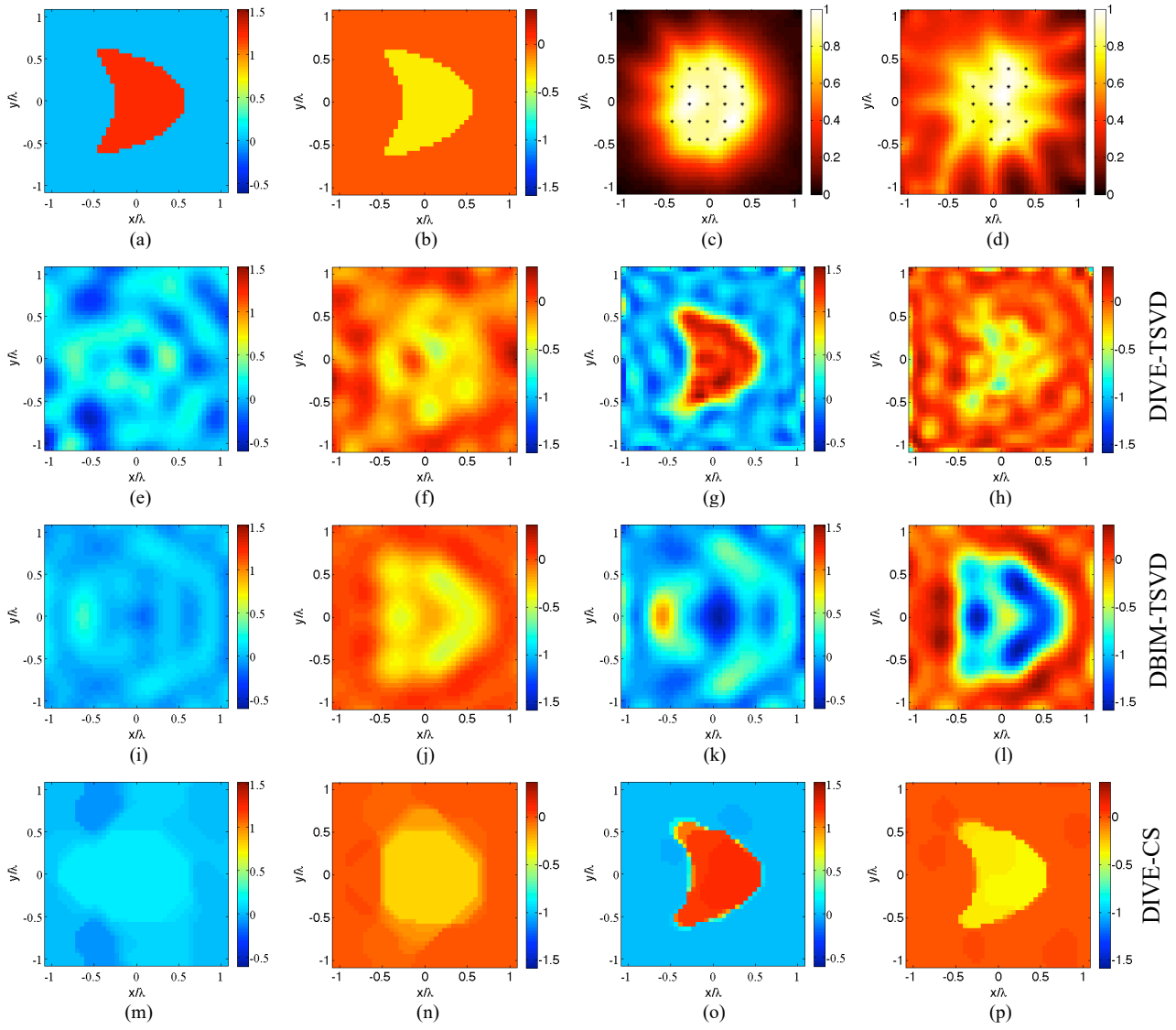


Fig. 2. The kite target: (a) real part and (b) imaginary part of the reference profile. Distorted LSM indicator (c) in the *Initialization* step and (d) for k = 1. Real part and imaginary part of the retrieved contrast function with DIVE-TSVD: (e)-(f) starting guess and (g)-(h) at final reconstruction. (i)-(l) and (m)-(p) are the same of (e)-(h) in the case of DBIM-TSVD and DIVE-CS, respectively.

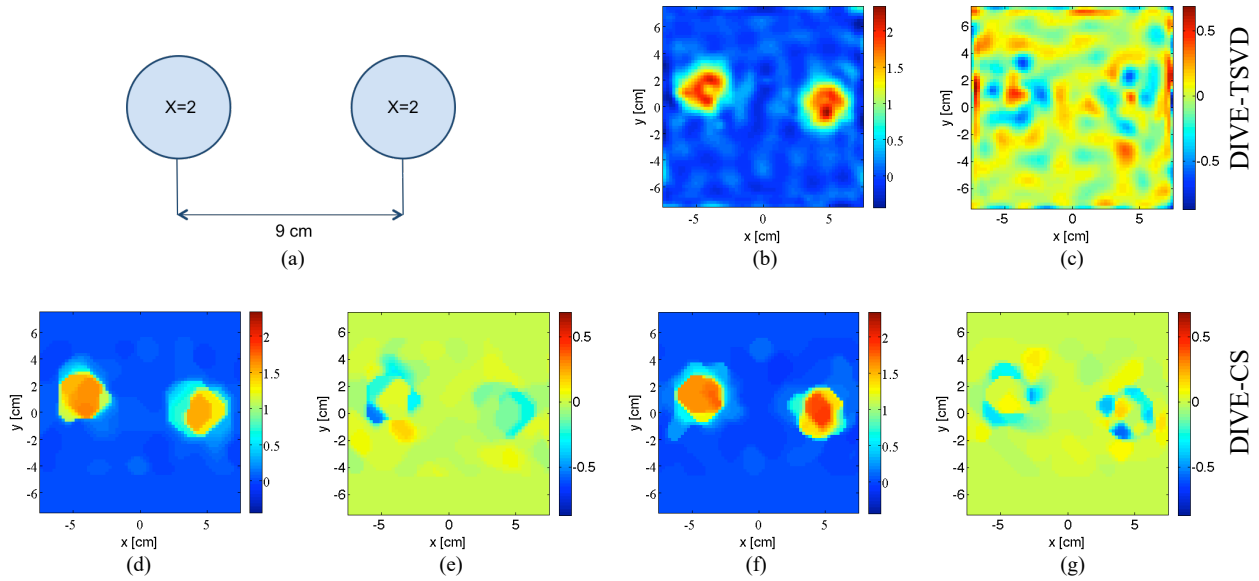


Fig. 3. The Fresnel *TwinDielTM* target at 6 GHz: (a) Reference profile. Real part and imaginary part of the retrieved contrast function with DIVE-TSVD (b)-(c) (during the iterative procedure $N_T$ = [140, 117, 90, 148, 106, 91, 126, 115, 154, 122, 131, 142]). (d)-(e) are the same of (b)-(c) in the case of DIVE-CS. (f)-(g) are the same of (d)-(e) for reduced number of processed data.

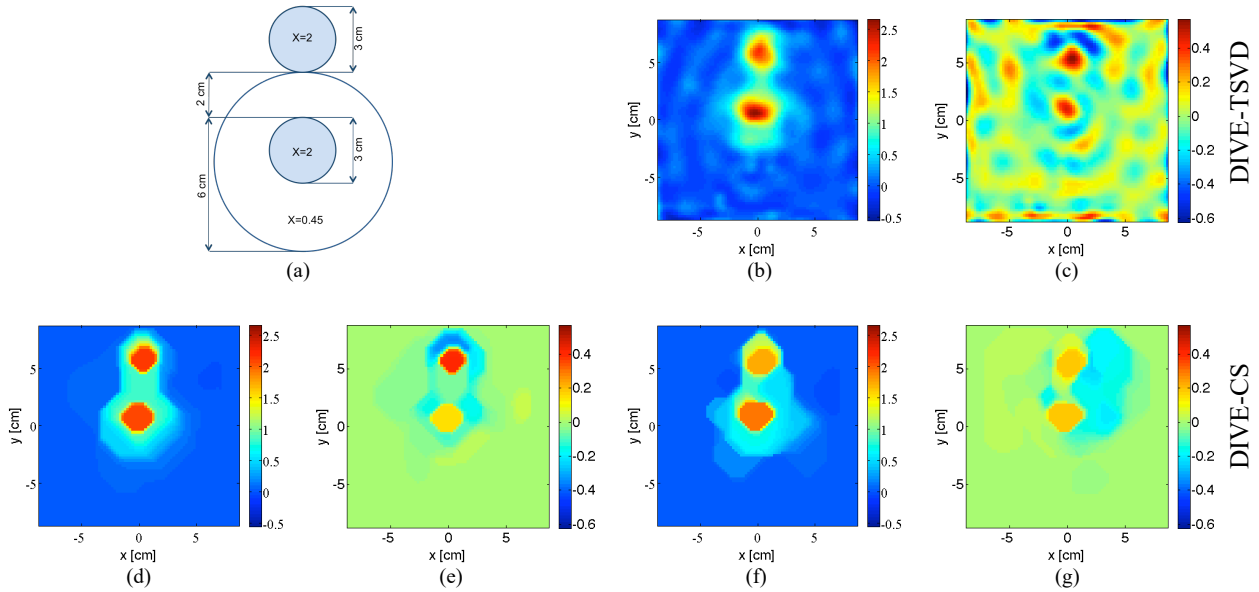


Fig. 4. The Fresnel *FoamTwinDielIntTM* target at 4 GHz: (a) Reference profile. Real part and imaginary part of the retrieved contrast function with DIVE-TSVD (b)-(c) (during the iterative procedure $N_T$ = [86, 86, 73, 96, 72, 50, 74, 34, 67, 68, 83, 69, 48]). (d)-(e) are the same of (b)-(c) in the case of DIVE-CS. (f)-(g) are the same of (b)-(c) for reduced number of processed data.

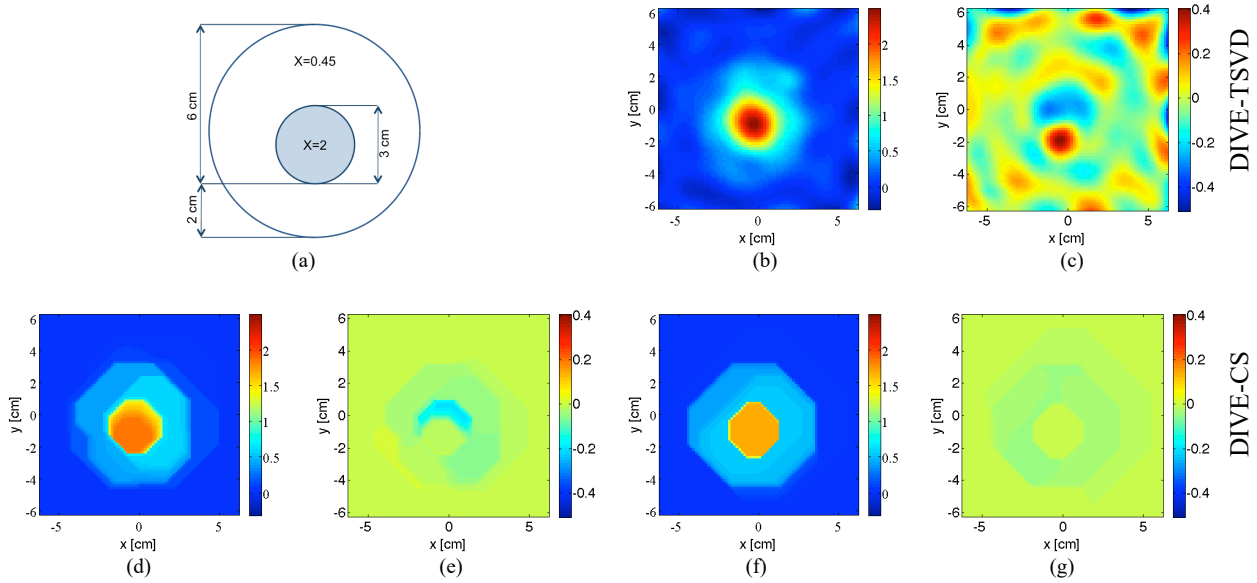


Fig. 5. TheFresnel *FoamDielIntTM* target at 4 GHz: (a) Reference profile. Real part and imaginary part of the retrieved contrast function with DIVE-TSVD (d)-(e) at the initial step and (f)-(g) at the last iteration (during the iterative procedure $N_T$ = [47, 55, 36, 51, 40, 47, 35, 46, 51, 55]). (h)-(k) are the same of (d)-(g) in the case of DIVE-CS and reduced number of processed data. (l)-(m) are the same of (j)-(k) for reduced number of processed data.

## VI. Conclusions

In this paper, a novel iterative approach for quantitative inverse scattering is introduced, described and assessed.

The proposed DIVE procedure consists in successive linearizations based on the virtual scattering experiments framework. In particular, at each iteration, on the basis of intermediate results, the relevant Green's function is updated, and the VE are re-designed to achieve convenient linearizations of the relationship between the (rearranged) data and the unknown dielectric and conductivity properties. This relationship is then used to refine at each step the contrast profile by solving the underlying ill-posed problem via CS or TSVD based inversions.

The DIVE-CS scheme allows to obtain nearly optimal reconstructions of extended but piecewise constant targets, which can be considered to be sparse when represented in terms of step functions. At each step, it involves the solution of a constrained optimization problem, which relies on an iterative procedure, so it is less computationally efficient with respect to DIVE-TSVD. On the other side, considerable advantages are gained in terms of the achieved spatial resolution, also due to the capability of enforcing at each step sparsity on the whole contrast profile. Moreover, a significant reduction of the number of antennas (and hence of the measurement apparatus complexity and the computational time) can be gained. In fact, one is able to achieve very accurate results also under aspect limited configurations and considering a reduced number of sensors with respect to all the existing literature.

Another interesting feature of DIVE, besides its much larger applicability as compared to the usual DBIM, is the fact that iterative linearizations allow to take profit in a simple way from the VE and CS paradigms, which is instead not the case when using non-linear inversion schemes, such as modified gradient [35] or contrast source inversion [36] approaches.

Results obtained by processing Fresnel experimental data have shown that DIVE, either using TSVD or CS, is actually capable of successfully imaging targets with just monochromatic data and without enforcing any kind of priori information on the admissible values of contrast profile. This is very relevant in all those cases (such as biomedical or subsurface imaging) where media are dispersive.

## References

[1] D. Colton and R. Kress. “Inverse Acoustic and Electromagnetic Scattering Theory”, *Springer-Verlag,* Berlin, Germany, 1998.

[2] M. Bertero and P. Boccacci. “Introduction to Inverse Problems in Imaging”, *Institute of Physics*, Bristol, UK, 1998

[3] A. J. Devaney, “Geophysical diffraction tomography,” *IEEE Trans. Geosci. Remote Sensing,* vol. GE-22, no. 1, pp. 3–13, 1984.

[4] A. J. Devaney, “Inverse scattering within the Rytov approximation,” *Opt. Lett.,* vol. 6, no. 8, pp. 374–376, 1981.

[5] A. J. Devaney and M. L. Oristaglio, “Inversion procedure for inverse scattering within the distorted-wave Born approximation,” *Phys. Rev. Lett.,* vol. 51, no. 4, pp. 237-240, 1983.

[6] W. C. Chew and Y. M. Wang, “Reconstruction of two-dimensional permittivity distribution using the distorted Born iterative method,” *IEEE Trans. Med. Imaging*, vol. 9, no. 2, pp. 218–225, 1990.

[7] C. Yu, M. Yuan, and Q. H. Liu, “Reconstruction of 3D objects from multi-frequency experimental data with a fast DBIM-BCGS method,” *Inverse Probl*., vol. 25, no. 2, p. 024007, 2009.

[8] C. Gilmore, P. Mojabi, and J. LoVetri, “Comparison of an enhanced distorted born iterative method and the multiplicative-regularized contrast source inversion method,” *IEEE Trans. Antennas Propag*., vol. 57, no. 8, pp. 2341–2351, 2009.

[9] T. J. Cui, W. C. Chew, A. A. Aydiner, and S. Chen, “Inverse scattering of two-dimensional dielectric objects buried in a lossy earth using the distorted Born iterative method,” *IEEE Trans. Geosci. Remote Sens*., vol. 39, no. 2, pp. 339–346, 2001.

[10] A. G. Tijhuis, K. Belkebir, A. C. S. Litman, and B. P. de Hon, “Multiplefrequency distorted-wave born approach to 2D inverse profiling,” *Inverse Probl*., vol. 17, no. 6, p. 1635, 2001.

[11] A. Desmal, and H. Bagci, "Shrinkage-Thresholding Enhanced Born Iterative Method for Solving 2D Inverse Electromagnetic Scattering Problem," *IEEE Trans. Antennas Propag*, vol. 62, no. 7, pp. 3878-3884, 2014.

[12] M. Azghani, P. Kosmas, F. Marvasti, "Microwave Medical Imaging Based on Sparsity and an Iterative Method With Adaptive Thresholding," *IEEE Trans. Medical Imaging*, vol. 34, no. 2, pp. 357-365, 2015.

[13] J. D. Shea, P Kosmas, S. C. Hagness, B. D. Van Veen, "Three-dimensional microwave imaging of realistic numerical breast phantoms via a multiple-frequency inverse scattering technique," *Med. Phys*., vol. 37, no. 8, pp. 4210-26, 2010.

[14] L. Crocco, I. Catapano, L. Di Donato and T. Isernia, "The linear sampling method as a way to quantitative inverse scattering," *IEEE Trans. Antennas Propag.*, vol. 60, no. 4, pp. 1844-1853, 2012.

[15] L. Di Donato, R. Palmeri, G. Sorbello, T. Isernia, and L. Crocco, "Assessing the capabilities of a new linear inversion method for quantitative microwave imaging," *Int. J. Antennas Propag.*, vol. 2015, no. ID:403760, 2015.

[16] L. Di Donato, M. Bevacqua, L. Crocco, and T. Isernia, "Inverse Scattering via Virtual Experiments and Contrast Source Regularization," *IEEE Trans. Antennas Propag,* vol. 63, no. 4, pp. 1669-1677, 2015.

[17] L. Di Donato, R. Palmeri, G. Sorbello, T. Isernia, and L. Crocco, "A New Linear Distorted Wave Inversion Method for Microwave Imaging via Virtual Experiments," under review on *IEEE Trans. Microw. Theory Techn*.

[18] D. Donoho, "Compressed sensing," *IEEE Trans. Inf. Theory*, vol. 52, no. 4, pp. 1289–1306, 2006.

[19] R. G. Baraniuk, "Compressive sampling," *IEEE Signal Process. Mag*., vol. 24, no. 4, pp. 118-124, 2007.

[20] E. J. Candès, M. Wakin, and S. Boyd. "Enhancing sparsity by reweighted l1 minimization," *J. Fourier Anal. Appl.*, vol.14, no. 5, pp. 877-905, 2008.

[21] L. Poli, G. Oliveri, and A. Massa, "Microwave imaging within the first-order Born approximation by means of the contrast-field Bayesian compressive sensing," *IEEE Trans. Antennas Propag.*, vol. 60, no. 6, pp. 2865–2879, 2012.

[22] M. Ambrosanio, and V. Pascazio, "A compressive-sensing-based approach for the detection and characterization of buried objects," *IEEE J. Sel. Topics Appl. Earth Observ. in Remote Sens.*, vol. 8, no. 7, pp. 3386–3395, 2015.

[23] O. M. Bucci and T. Isernia, "Electromagnetic inverse scattering: Retrievable information and measurement strategies," *Radio Sci.*, vol. 32, no. 6, pp. 2123–2138, 1997.

[24] D. Colton, H. Haddar, and M. Piana, "The linear sampling method in inverse electromagnetic scattering theory," *Inv. Probl*., vol. 19, no. 6, pp. 105–137, 2003.

[25] I. Catapano and L. Crocco, "An imaging method for concealed targets," *IEEE Trans. Geosci. Remote Sens*., vol. 47, no. 5, pp. 1301–1309, 2009.

[26] P. C. Hansen, "The discrete picard condition for discrete ill-posed problems," *BIT Numer. Math.*, vol. 30, no. 4, pp. 658–672, 1990.

[27] P. C. Hansen and D. P. O'Leary, "The use of L-curve in the regularization of discrete ill-posed problem," *SIAM J. Sci. Comput*., vol. 14, no. 6, pp. 1487–1503, 1993.

[28] M. Bevacqua, L. Crocco, L. Di Donato, and T. Isernia, "Microwave imaging of non-weak targets via compressive sensing and virtual experiments," *IEEE Antennas Wireless Propag. Letters*, vol. 14, pp. 1035–1038, 2015.

[29] M. Bevacqua, and L. Di Donato, "Improved TV-CS approaches for inverse scattering problem," *Scientific World J.*, vol. 2015, no. ID:262985, 2015.

[30] J. Richmond, "Scattering by a dielectric cylinder of arbitrary cross section shape," *IEEE Trans. Antennas Propag*., vol. 13, no. 3, pp. 334-341, 1965.

[31] K. Belkebir and M. Saillard, "Special section: Testing inversion algorithms against experimental data," *Inverse Probl*., vol. 17, no. 6, pp. 1565–2028, 2001.

[32] K. Belkebir and M. Saillard, "Special section: Testing inversion algorithms against real data: Inhomogeneous targets," *Inverse Probl*., vol. 21, no. 6, 2005.

[33] A. Abubakar, P. M. van den Berg, and T. M. Habashy. "Application of the multiplicative regularized contrast source inversion method on TM- and TE-polarized experimental Fresnel data," *Inverse Probl.*, vol. 21, no. 6, S5-S13, 2005.

[34] L. Crocco, M. D'Urso, and T. Isernia. "Testing the contrast source extended Born inversion method against real data: the TM case," *Inverse Probl.,* vol. 21, no. 6, S33, 2005

[35] R. E. Kleinman, and P. M. van den Berg, "A modified gradient method for two-dimensional problems in tomography," *J. Comp. Appl. Math.,* vol. 42, no.1, pp. 17-35, 1992.

[36] P. M. Van Den Berg, and R. E. Kleinman. "A contrast source inversion method," *Inverse Probl.*, vol. 13, no. 6, 1997.